

HPC4EI: Simulation of Microstructure Evolution of Battery Electrode Drying Process

(DOE Award DE-AC05-76RL01830 CRADA 619)

Objective: to predict dried electrode microstructure, binder migration, and debonding to provide science-based guideline toward minimizing drying time and/or energy with improved electrode quality

Xinxin Yao and Lei Chen, University of Michigan – Dearborn

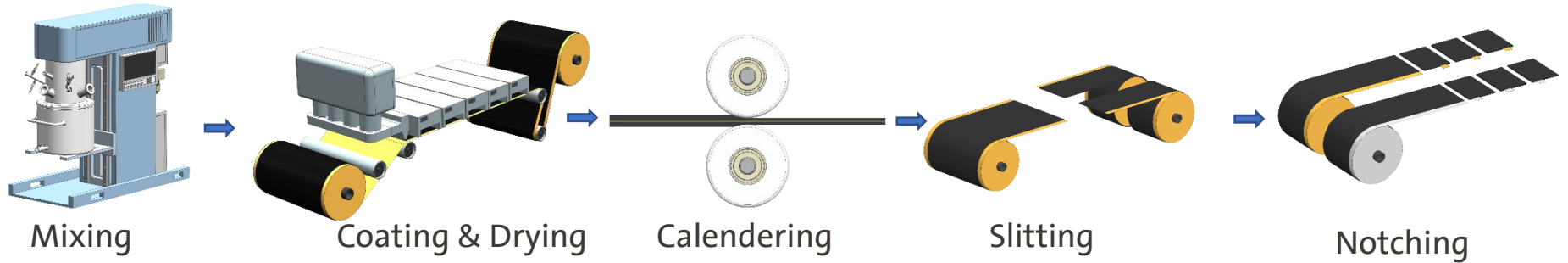
Wayne Cai, Hasnain Hafiz and Yangbing Zeng, General Motors LLC

Zirui Mao and Shenyang Hu, Pacific Northwest National Laboratory

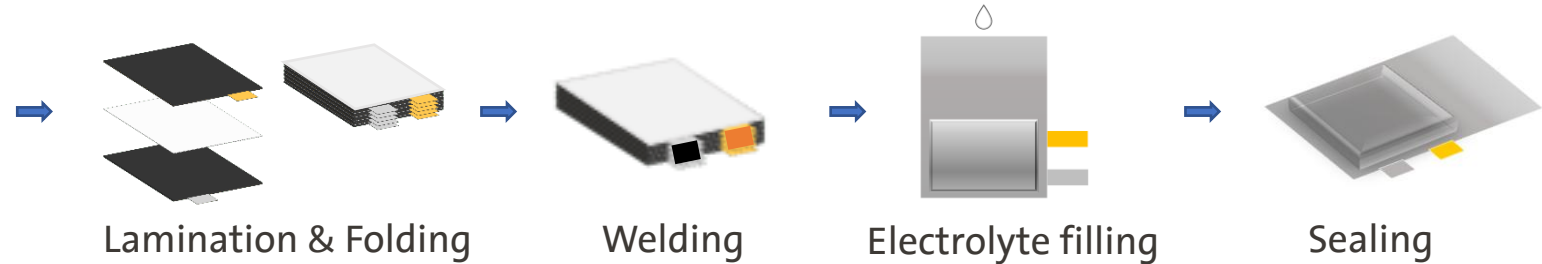
January 24, 2026

Battery Cell Manufacturing Processes

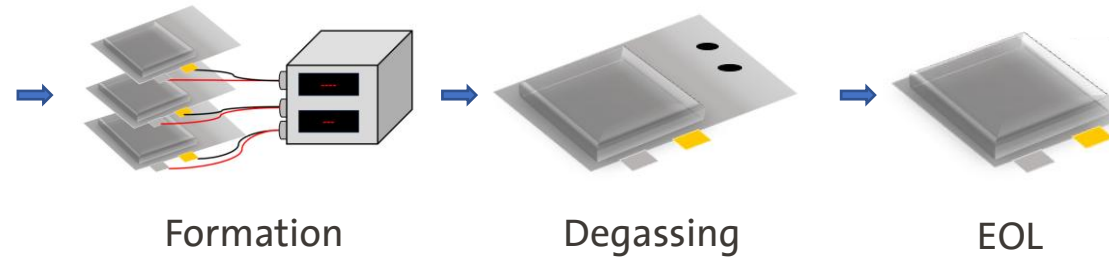
ELECTRODE	Mixing
	Coating
	Drying
	Calendering
	Slitting
	Notching



ASSEMBLY	Lamination
	Folding
	Welding
	Electrolyte fill
	Sealing



FORMATION	Formation
	Degassing
	EOL



Electrode Drying Process

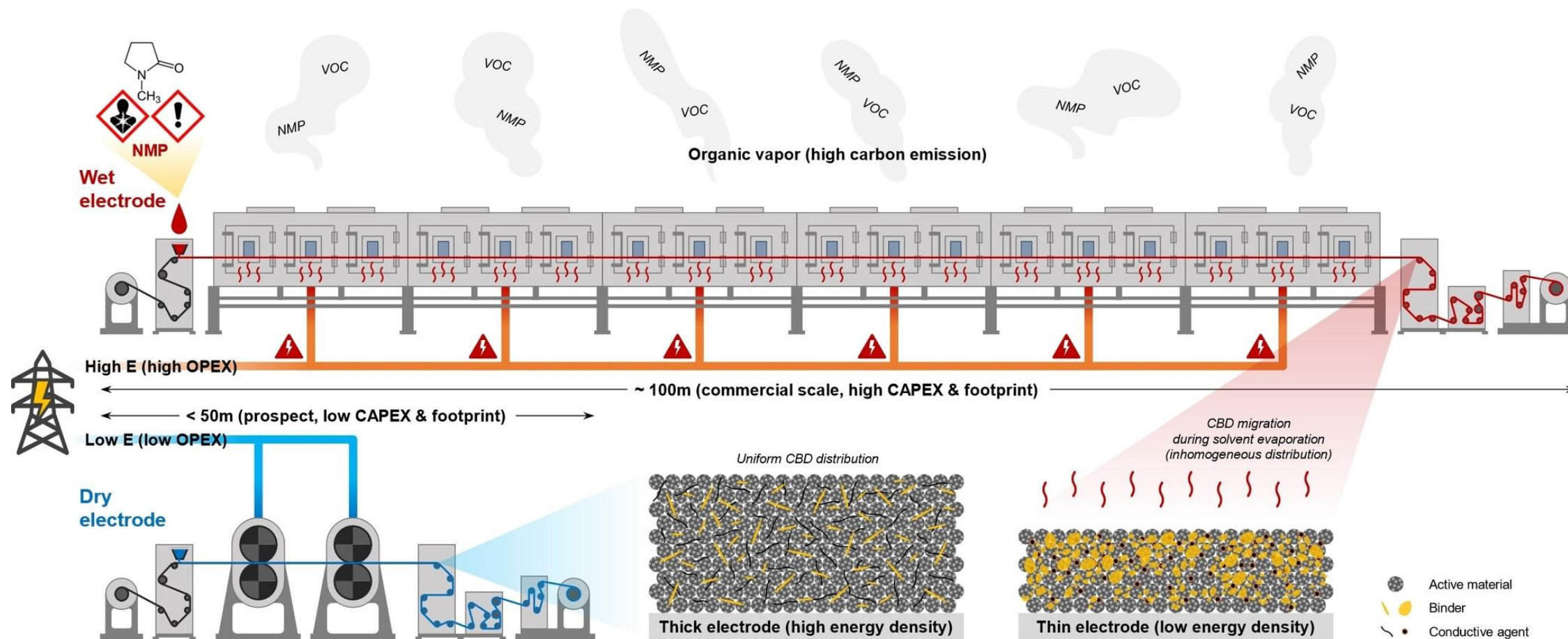


Fig. 2 Schematic overview comparing wet and dry electrode manufacturing lines. The top illustrates the traditional wet process with substantial equipment footprint and VOC/NMP emissions, leading to inhomogeneous binder distribution. The bottom shows the streamlined dry process with a smaller footprint, lower CAPEX, and the production of thicker electrodes with uniform composition, enabling higher energy densities.

ChemElectroChem: Volume 11, Issue 17, 2024, <https://doi.org/10.1002/celc.202400288>

Energy Impact: Drying Process Consumes ~47% of Total Energy Consumption

Table 1. Cost, throughput, and energy consumption of LIB manufacturing processes

Manufacturing processes	Cost per year/\$* (Nelson et al., 2019)	Percentage %	Throughput (Heimes et al., 2019a)	Manufacturing processes	Energy consumption per cell/kWh	Percentage %
Slurry mixing	7,396,000	7.91%	30 min–5 h	Slurry mixing	0.11	0.83%
Coating/drying	13,984,000	14.96%	35–80 m/min	Coating	0.18	1.36%
Solvent recovery	4,296,000	4.60%	NA	Drying/solvent recovery	6.22	46.84%
Calendering	4,849,000	5.19%	60–100 m/min	Calendering	0.38	2.86%
Slitting	2,891,000	3.09%	80–150 m/min	Slitting	0.71	5.35%
Vacuum drying	2,990,000	3.20%	12–30 h	Stacking	0.77	5.80%
Stacking	8,086,000	8.65%	NA	Welding	0.25	1.88%
Welding	6,864,000	7.34%	NA	Enclosing	0.69	5.20%
Enclosing	11,636,000	12.45%	Depend on the cell design	Formation/aging	0.07	0.53%
Formation/aging	30,482,750	32.61%	Up to 1.5–3 weeks	Dry room	3.9	29.37%

*The manufacturing cost includes equipment depreciation, labor cost, and plant floor space cost.

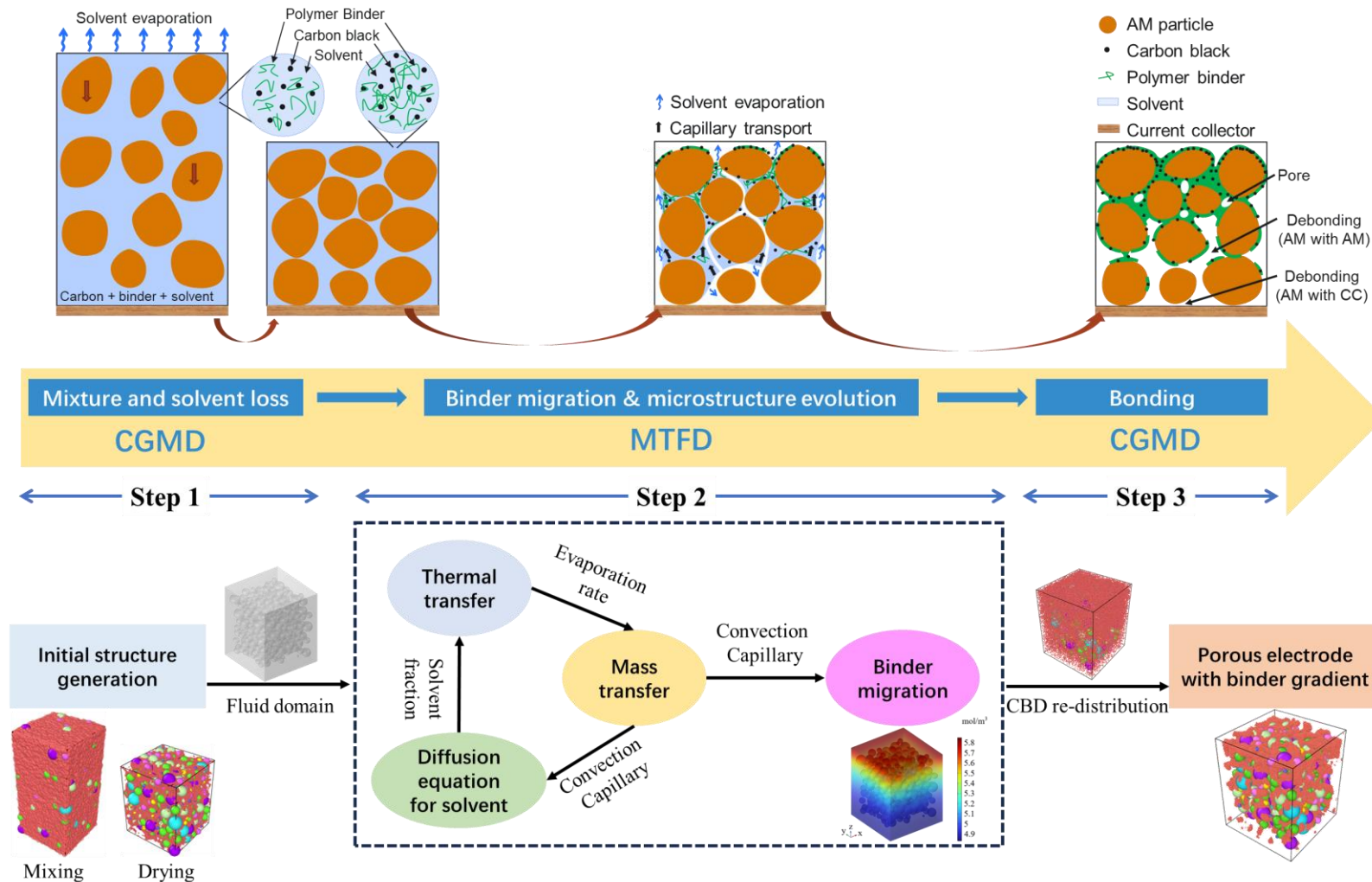
The labor cost was calculated based on the US average factory worker's salary of \$15/h (Economic Research Institute, 2020).

The floor space cost was calculated based on \$3,000/m² per year (includes rent, utility, and management) (Nelson et al., 2019).

The depreciation cost was calculated by 16.7% of capital investment and 5% of floor space cost (Nelson et al., 2019).

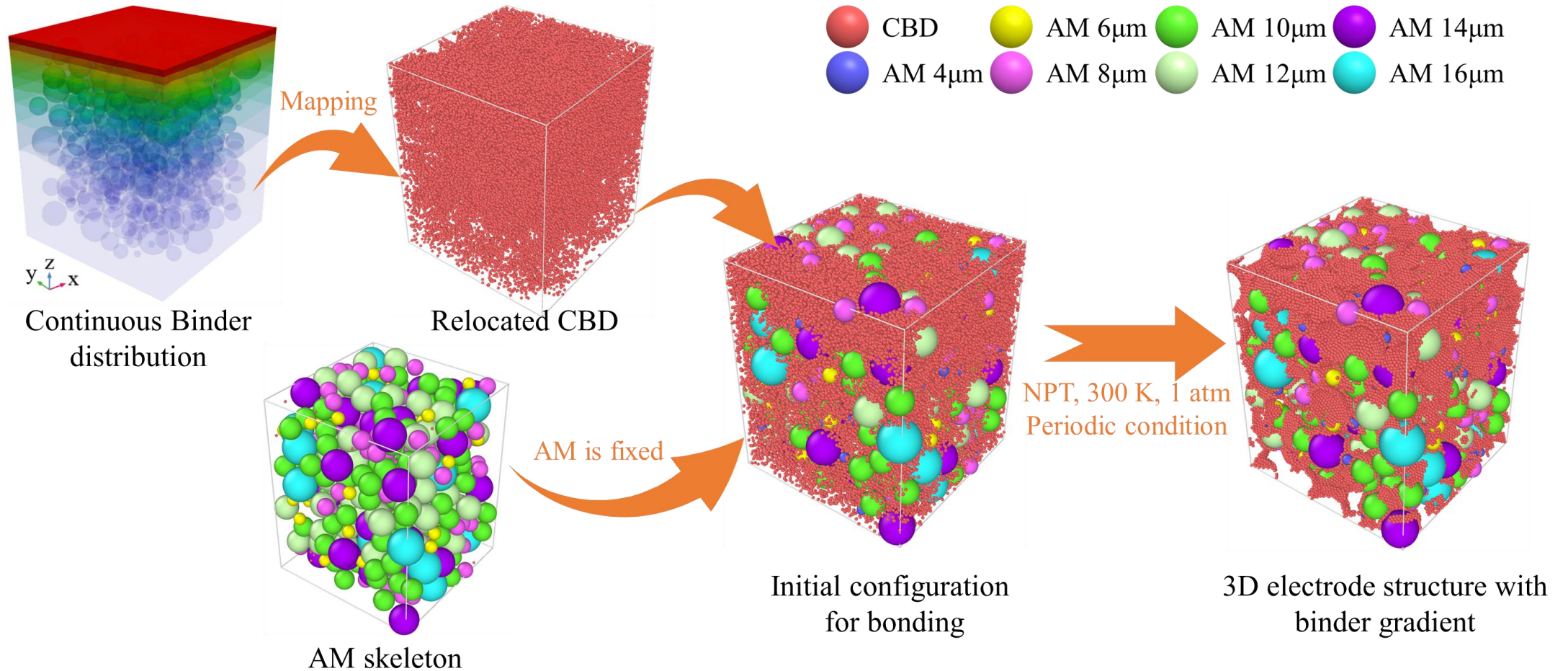
Y.T. Liu, et al., Current and future lithium-ion battery manufacturing, iScience, 2021.

Computational Model #1: CGMD

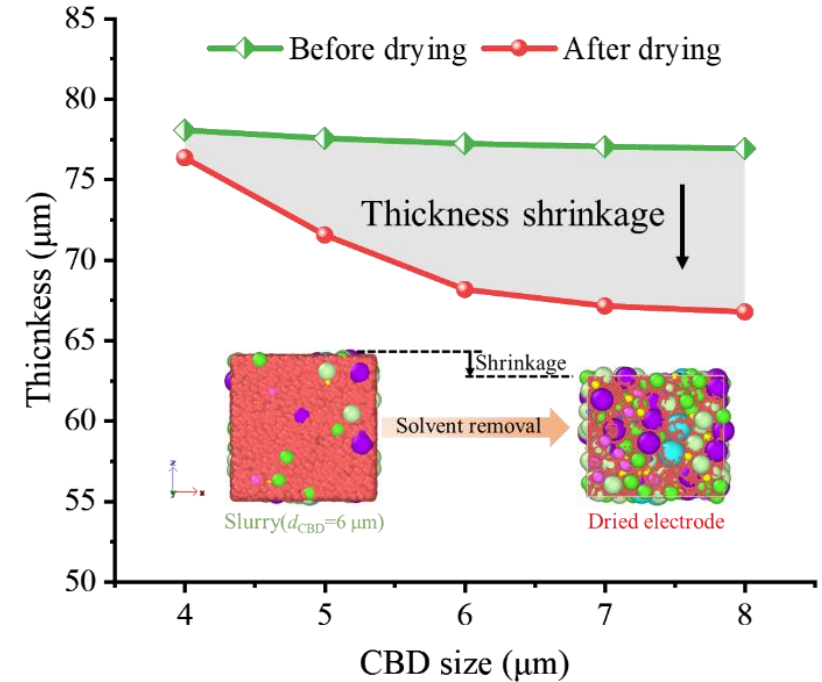
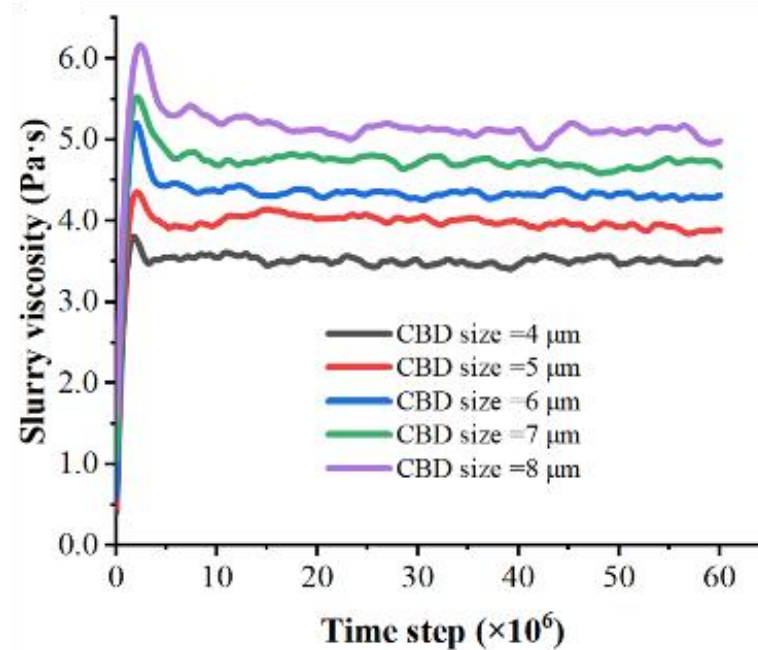
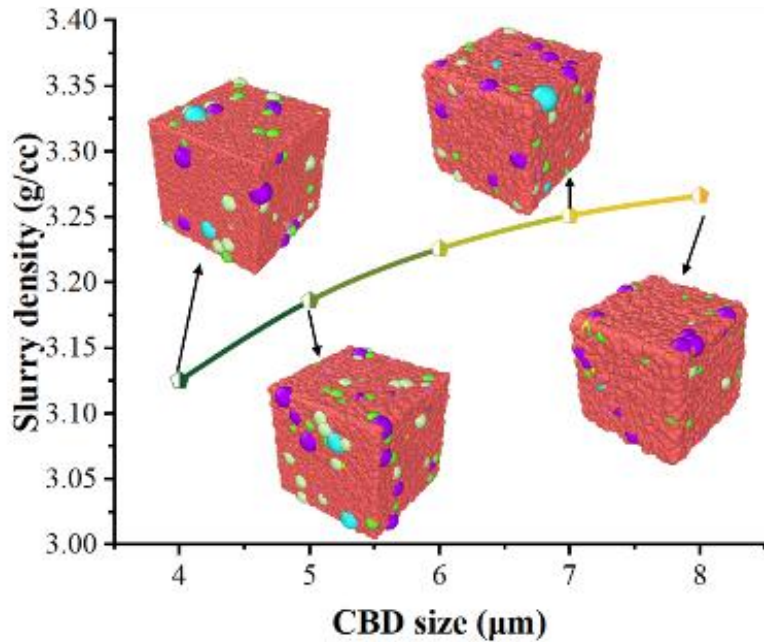


- **LAMMPS (Large-scale Atomic/Molecular Massively Parallel Simulator)** is used for Coarse Grained Molecular Dynamics (CGMD) simulation
- **COMSOL** is used for thermal/CFD simulation

Computational Model #1: CGMD

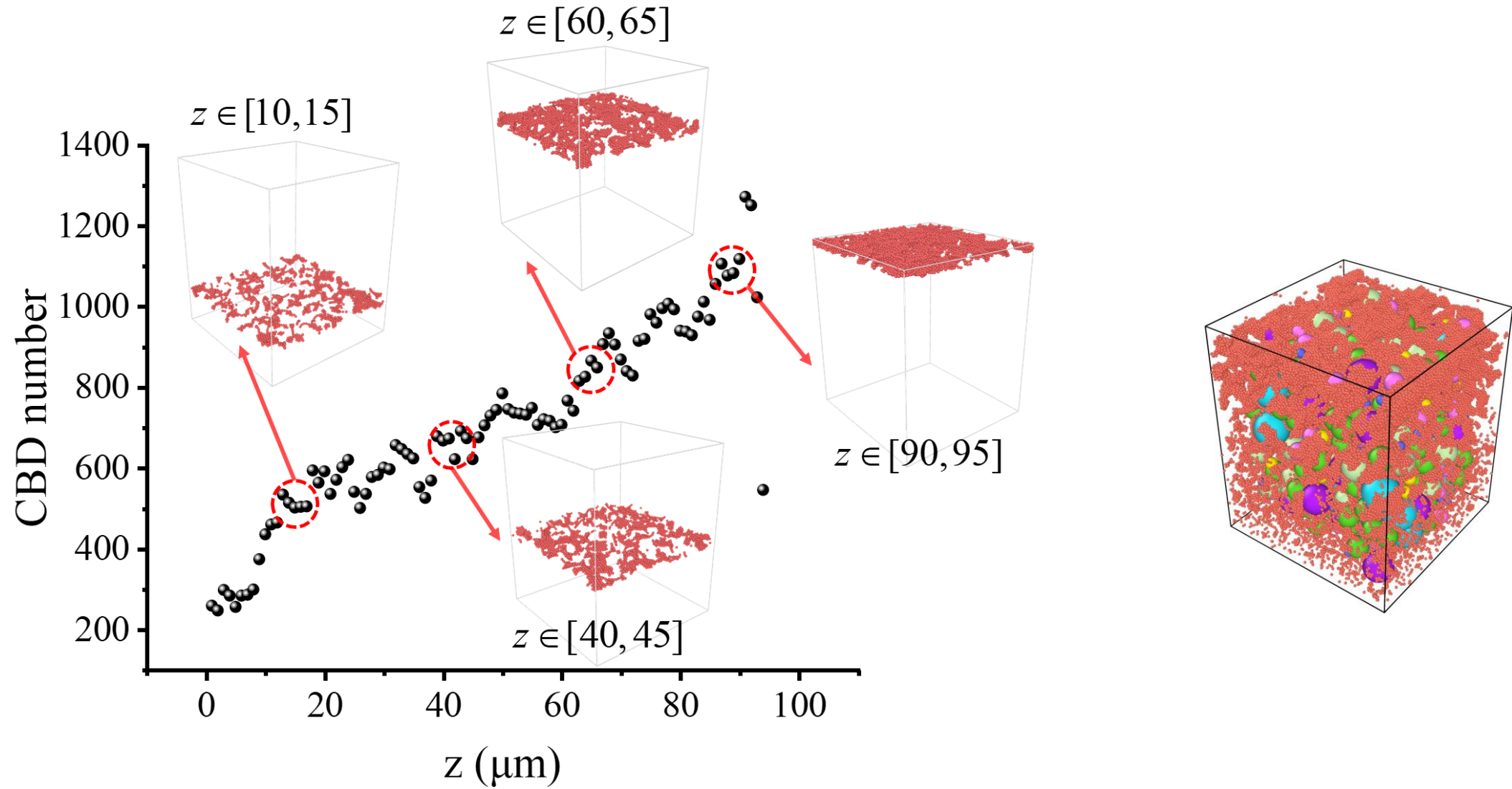


Computational Model #1: Sensitivity Analysis



- The CBD size and the density greatly influence physical properties such as density, viscosity, thickness and porosity.

Computational Model #1: Binder Migration



Computational Model #1: Computational Cost

Slurry mixing- different CBD size

CBD density	CBD size	Low	High	Domain Size (μm)	Volume (μm^3)	Mass (pg)	Slurry density (g/cc)	Atoms	Types	Wall Time (hour)	Cores	Resource
0.1	4	460.98	539.02	78.04	475282.4545	1485473	3.125453056	125960	8	19.1	64	1222.4
0.1	5	461.23	538.77	77.54	466205.4971	1485473	3.186305201	64750	8	8.5	64	544
0.1	6	461.39	538.61	77.22	460457.331	1485473	3.226081767	37700	8	4.3	64	275.2
0.1	7	461.49	538.51	77.02	456888.8324	1485473	3.251278855	23940	8	2.4	64	153.6
0.1	8	461.55	538.45	76.9	454756.609	1485473	3.26652317	16210	8	1.44	64	92.16
												2287.36

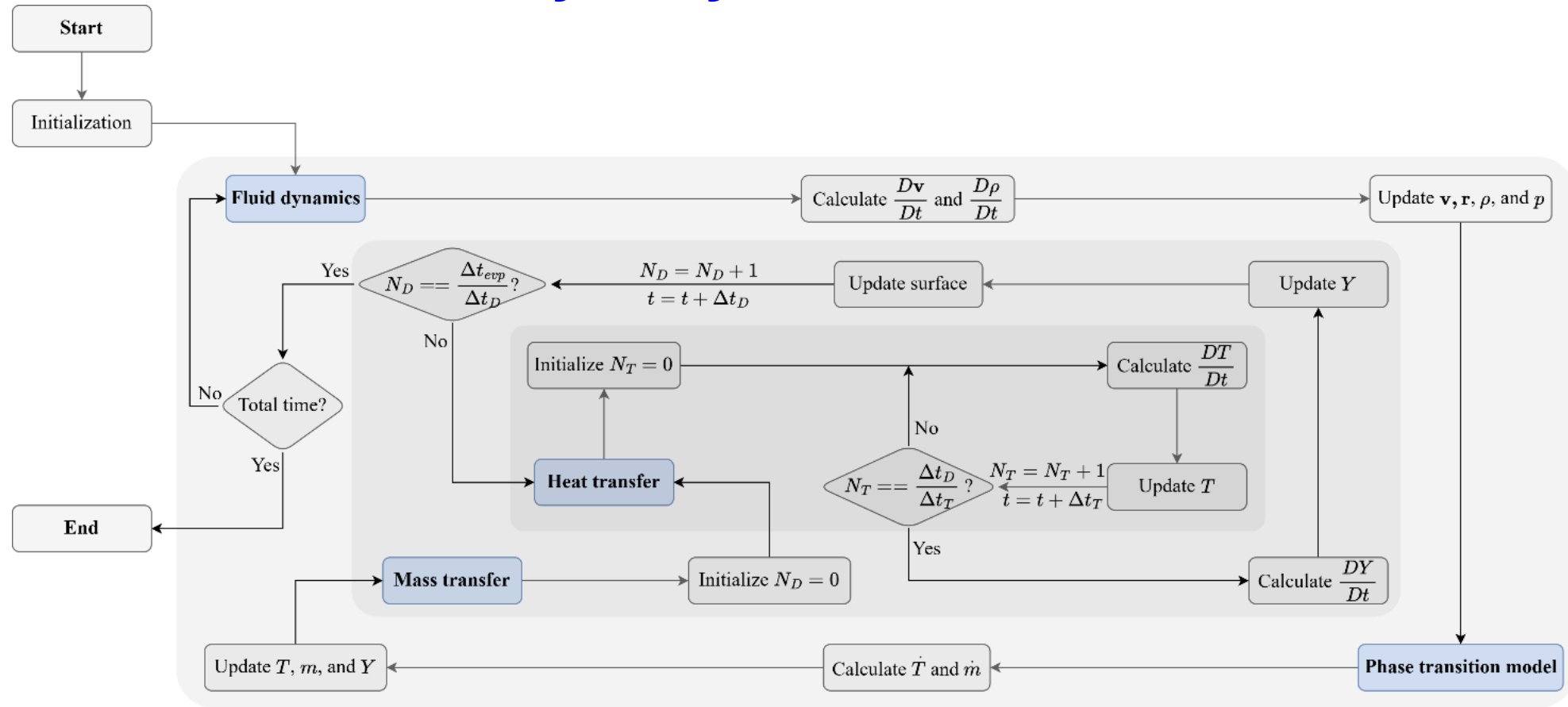
Slurry mixing- different CBD density

CBD density	CBD size	Low	High	Domain Size (μm)	Volume (μm^3)	Mass (pg)	Slurry density (g/cc)	Atoms	Types	Wall Time (hour)	Cores	Resource
0.04	6	448.3	551.69	103.39	1105186.588	1485473	1.344092496	93440	8	8.9	64	569.6
0.06	6	454.63	545.37	90.74	747130.2572	1485473	1.98823831	62480	8	6.5	64	416
0.08	6	458.6	541.4	82.8	567663.552	1485473	2.616819408	46990	8	5.2	64	332.8
0.1	6	461.39	538.61	77.22	460457.331	1485473	3.226081767	37700	8	4.3	64	275.2
0.12	6	463.51	536.49	72.98	388697.3476	1485473	3.82167002	31500	8	4	64	256
0.14	6	465.19	534.81	69.62	337444.2691	1485473	4.402128398	27080	8	3.5	64	224
												2073.6

Slurry mixing- different AM particle size selection

CBD density	CBD size	Low	High	Domain Size (μm)	Volume (μm^3)	Mass (pg)	Slurry density (g/cc)	Atoms	Types	Wall Time (hour)	Cores	Resource
0.1	6	459.89	540.11	80.22	516235.6266	1485473	2.877509655	37693	6	4.5	64	288
0.1	6	461.39	538.61	77.22	460457.331	1485473	3.226081767	37700	8	4.3	64	275.2
0.1	6	461.39	538.61	77.22	460457.331	1485473	3.226081767	37701	14	4.4	64	281.6
												844.8

Computational Model #2: Smoothed-Particle Hydrodynamics (SPH)



Flowchart of the three-level time stepping SPH framework illustrating the synchronization of processes with widely varying rates during drying.

Computational Model #2: Smoothed-Particle Hydrodynamics (SPH)

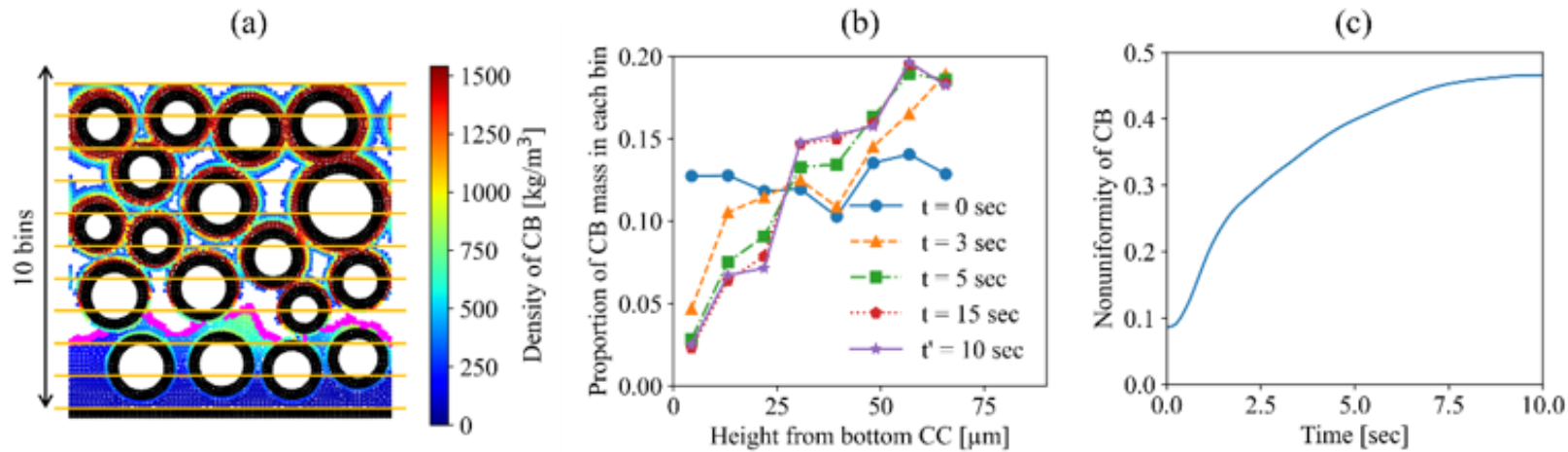


Figure 20 CB distribution in depth after dried obtained from SPH modelling. (a) Subdivision of the system into ten bins for quantitative analysis. (b) Spatial distribution of CB across vertical bins at different time points. (c) Evolution of non-uniformity (η_{CB}) in CB vertical distribution, calculated by

$$\eta_{CB} = \frac{\sqrt{\frac{1}{N_{bin}} \sum_{i=1, N_{bin}} (m_i - \bar{m})^2}}{\bar{m}}$$
, where N_{bin} is the total number of bins, m_i is the total mass of CB within the i -th bin, and \bar{m} is the average mass across the domain. Zero η means uniformity.